Energy Proceedings
Vol 35, 2023
ISSN 2004-2965

Study on Transport Mechanism of CO_2-CH_4 Binary System in Coalbed Methane Reservoir Nanopore with Multiple Inducement Deformation Field

Xiangji Dou[1*], Pengfei Zhu[1],Zhengdong Lei[2],Nan Pan[1],Run Duan[1],Luyao Guo[1]

1 Changzhou University

2 PetroChina Research Institute of Petroleum Exploration and Development
(dxj@cczu.edu.cn)

ABSTRACT

Shale gas, as a strategic supplement to conventional oil and gas resources, has become the focal point of China's oil and gas exploration and development. CO_2 huff and puff, a pivotal technique in shale gas exploitation, not only effectively enhances shale gas recovery but also aligns with the goal of carbon neutrality. The nano-scale phenomena of CO_2-multi-component gas micro-mobility extensively occur during the CO_2 huff and puff process in shale gas reservoirs. Under the coupled variable conditions within the pore structure, the adsorption characteristics and storage state of the gas within the pores also change. This paper uses molecular simulation methods to study the adsorption characteristics of mixed gases in synergistically deforming organic nanopores, as well as the transport mechanism of mixed gases in inorganic nanopores of shale. The research found that when CO_2 has the maximum proportion, the deformation is greater than at other proportions, and the maximum deformation at different proportions all occur at 5MPa. With the increase of the initial pore diameter, the amplitude of pore deformation also increases. When gas molecules begin to move in the pores, the change in cohesive energy will provide some resistance. However, when gas molecules stably move in the pores, the resistance effect produced by the cohesive energy will relatively weaken. The pore diameter at the nano-scale will change under the influence of the water film. If this effect is ignored, it will lead to a significant deviation in the calculation results of capillary pressure.

Keywords:
Shale Gas; Molecular Simulation; Adsorption Characteristics; Mobility

NONMENCLATURE

λ *represents the average molecular mean free path (nm) ;*

D *represents the characteristic length is the pore diameter (nm) ;*

K *represents the permeability of shale under effective stress (m²);*

P_e *represents the intrinsic permeability of shale under atmospheric pressure (m²);*

P_o *symbolizes effective stress (MPa) ;*

ϕ *represents atmospheric pressure (MPa) ;*

ϕ_o *represents the porosity of shale under effective stress (dimensionless);*

s represents the stress deformation coefficient of shale permeability (dimensionless) ;

q represents the stress deformation coefficient of shale porosity (dimensionless) ;

r_o *represents the initial pore radius of shale pores (nm) ;*

r_{iom} *represents the pore radius under effective stress in shale inorganic nanopores (nm) ;*

δ *represents the thickness of the water film (nm) ;*

$\phi_{e\text{-}iom}$ *represents the effective porosity (dimensionless) ;*

$r_{e\text{-}iom}$ *represents the effective pore radius (nm) ;*

This is a paper for International CCUS Conference 2023 (ICCUSC2023), April 14-15, 2023, Beijing, China.

μ *represents the gas viscosity (Pa·s) ;*

P *represents pore pressure (MPa) ;*

Z *represents the gas compressibility factor (dimensionless) ;*

M *represents the molar mass of the gas (kg/mol) ;*

R *designates the gas constant (J/(mol·K)) ;*

T *represents the formation temperature (K) ;*

P_{pr} *represents the comparative pressure of the gas (dimensionless) ;*

T_{pr} *represents the comparative temperature of the gas (dimensionless) ;*

P_c *represents the critical pressure (MPa) ;*

T_c *represents the critical temperature (K) ;*

λ_{mix} *represents the average molecular mean free path of the multicomponent gas mixture (nm) ;*

μ_{mix} *represents the viscosity of the multicomponent gas mixture (Pa·s) ;*

M_{mix} *represents the molar mass of the multicomponent gas mixture (kg/mol) ;*

Z_{mix} *represents the compressibility factor of the multicomponent gas mixture (dimensionless) ;*

J_D *represents the mass flow rate of slip flow at the no-slip boundary under the influence of a pressure gradient (kg/(m²·s)) ;*

K_∞ *represents the inherent permeability of the porous medium (m²) ;*

ϕ *represents porosity (dimensionless),* μ *represents gas viscosity (Pa·s) ;*

ρ *represents gas density (kg/m³) ;*

P *represents pore pressure (MPa) ;*

r *represents pore radius (nm) ;*

L *represents pore length (nm) ;*

b *represents the slip constant (dimensionless) ;*

J_k *represents the Knudsen diffusion mass flow rate (kg/(m²·s));*

C *represents the gas concentration (mol/m³);*

D_k *represents the Knudsen diffusion coefficient (m²/s) ;*

$\omega_{v\text{-iom}}$ *represents the weight coefficient of slip flow permeability for multicomponent gases in inorganic nanopores (dimensionless);*

$K_{v\text{-iom}}$ *represents the slip flow permeability for multicomponent gases in inorganic nanopores (m²);*

$\omega_{k\text{-iom}}$ *represents the weight coefficient of Knudsen diffusion permeability for multicomponent gases in inorganic nanopores (dimensionless);*

$K_{k\text{-iom}}$ *represents the Knudsen diffusion permeability for multicomponent gases in inorganic nanopores (m²).*

1. INTRODUCTION

Due to the abundant reserves of shale gas, its exploration and development are of utmost importance worldwide. It is generally recognized that there exist significant disparities in the storage conditions and content of shale gas within shale reservoirs. The CO_2 huff and puff in shale gas reservoirs not only improves the recovery rate of shale oil but also effectively sequesters CO_2, achieving the purpose of controlling CO_2 emissions.

However, during the process of shale gas reservoir development using CO_2 huff and puff, the pore pressure field (hereinafter referred to as the pore pressure) within the shale reservoir changes due to the injection and output of the fluid. This leads to alterations in the adsorption characteristics and pore throat structure; moreover, complex coupling and synergistic effects exist between the pore pressure, adsorption characteristics, and nano pore throat deformation field (hereinafter referred to as the deformation field). The relationships among these factors are intricate: the changes in adsorption characteristics are the result of the synergistic effects of the pore pressure and the deformation field; the deformation field is caused by the synergistic effects of the pore pressure and adsorption characteristics, and there is a coupling effect between the deformation field and adsorption characteristics. The

coupling and synergistic effects of the pore pressure, adsorption characteristics, and deformation field lead to dynamic changes in microscopic properties of shale nanopores, such as pore pressure, true pore diameter, and phase migration radius, thereby forming a dynamic nanopore effect.

On the other hand, the migration of gas in nano-scale pores is greatly restricted. This is due to the powerful interaction forces between gas molecules and between gas molecules and the pore wall, resulting in substantial resistance to the migration of gas in nanopores, thus rendering gas mobility poor. However, there exist numerous issues in the current research. For instance, the study of shale gas migration based on a single component does not fully represent the properties of shale gas. Some simulation studies apply constant force to gas molecules but cannot satisfy reservoir conditions. Traditional experimental research for analyzing gas migration in nanopores has significant limitations such as observation inconvenience and difficulties in revealing mechanisms. These challenges have led to slow progress in the study of shale gas migration in nanopores, thereby necessitating the establishment of a new technical method suitable for shale gas reservoirs to elucidate the behavior and dynamical mechanisms of shale gas migration in nanopores. Therefore, this paper adopts the molecular dynamics simulation method that can conveniently and intuitively reveal the microscopic mechanism of gas migration. We selected multi-component alkane molecules to study the gas migration process, and used the stretched molecular dynamics simulation method to achieve the over-pressure drive mode of shale gas migration. The research investigates the migration behavior and dynamical mechanisms of CO_2-multi-component gas in inorganic nanopores of shale, uncovers the dynamic process of gas migration in nanopores, reveals the resistance response mechanism during the gas migration process, and analyzes the influence of factors such as water film thickness, gas-water inter-facial tension on capillary pressure.

2. ADSORPTION CHARACTERISTICS OF MIXED GAS IN SYNERGISTICALLY DEFORMED ORGANIC NANOPORES

2.1 Model Establishment

A single crystal cell structure of graphene is imported from the Material Studio software database. Through the super cell module, we construct a super cell model with lattice parameters of a=49.2Å, b=42.6Å, α=90°, β=90°, γ=120° ($20a_0 \times 10b_0 \times 1c_0$). We obtain a single layer of graphene through the cleave surface and build an initial graphene slit model for simulation with a vacuum of 100 Å through the build layers. The width of the vacuum layer corresponds to the size of the pore diameter, with an initial pore diameter of 10Å. Given that this model is fixed in the Z-axis direction and open in the X-axis and Y-axis directions, it represents a layered structure. Hence, we employ periodic boundary conditions in the X and Y directions, infinitely repeating in space to simulate the macroscopic system of the shale reservoir. Because this layered structure is supported by other parts of the rock mass, it can be regarded as a rigid structure. As shown in Fig.1, during adsorption simulation, for the sake of simplified calculations, the model is fixed, and only deformation in the Z direction is considered, neglecting deformation in the X and Y directions caused by adsorption.

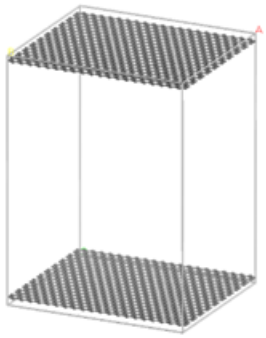

Fig.1 Organic nano pore structure

2.2 Method of calculation

Simulations employ the Sorption module in Materials Studio. Specific parameter settings include: the Metropolis method of the grand canonical Monte Carlo is selected; the Fixed Pressure task is adopted, with a designated fixed pressure; the COMPASS force field is utilized for simulation; system pressure ranges from 0 to 30 MPa, with pressure points at 0.1 MPa, 5 MPa, 10 MPa, 15 MPa, 20 MPa, 25 MPa, and 30 MPa; temperature ranges from 333K to 433K; model pore diameter ranges from 20 to 100Å; the molar ratio of components is set at (3:1:1:1/3:1:1:1); and both production and equilibrium steps are 2×10^6 . The van der Waals interaction between molecules is calculated using the Atom summation method, and the electrostatic interaction is calculated using the Ewald summation method, with a cut-off radius of 12.5Å. The model system under study is of periodic boundaries. Based on this, multiple simulation experiments are conducted, and the average value is taken. Below is a map of the equilibrium adsorption structure.

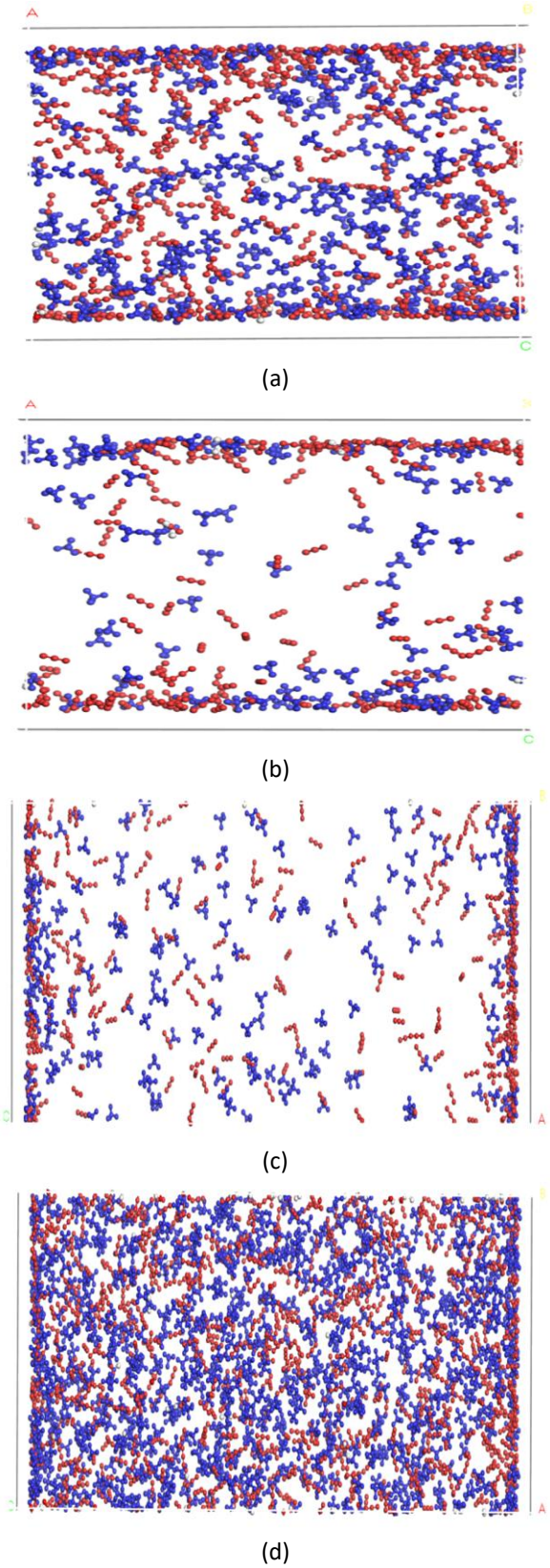

(a)

(b)

(c)

(d)

Fig.2 Conceive a map of the Song Dynasty in an instant

2.3 Results Analysis

2.3.1 Variation with Temperature

Overall, the trend of deformation quantity increases as pressure decreases. As the temperature rises from low to high, the maximum deformation of the pore gradually decreases. At 333K, the maximum deformation reaches 31.76%, while at 433K, the maximum adsorption quantity reaches 25.94%. Moreover, for deformation quantities at different temperatures, the fastest-growing pressure interval varies. For instance, from 30 to 15MPa, the deformation order is 433k>413k>393k>373k>353k>313k. Conversely, when the pressure is between 5 and 15MPa, the deformation order is reversed. Because the calculation formula of deformation quantity primarily depends on the difference in adsorption quantity, the difference in fugacity, and temperature. According to previous studies, as temperature increases, adsorption quantity decreases. Therefore, at lower temperatures, the primary influencing factor is adsorption quantity (i.e., the difference in adsorption quantity). When the temperature increases, the primary influencing factor gradually changes to the difference in fugacity.

As can be clearly seen from Fig.3, at 25MPa, the deformation quantity at 333K is 3.21%, while it is 6.97% at 433K. However, when the pressure decreases to 5MPa, the deformation quantity at 333K reaches its maximum of 31.76%, and it is 25.94% at 433K, a difference of 5.82%. Overall, the deformation quantity of pores decreases as temperature increases. According to the deformation quantity formula, deformation mainly depends on temperature, fugacity, and deformation quantity. For the same pore diameter, pressure, and different temperatures, the main dependent factor of deformation quantity changes.

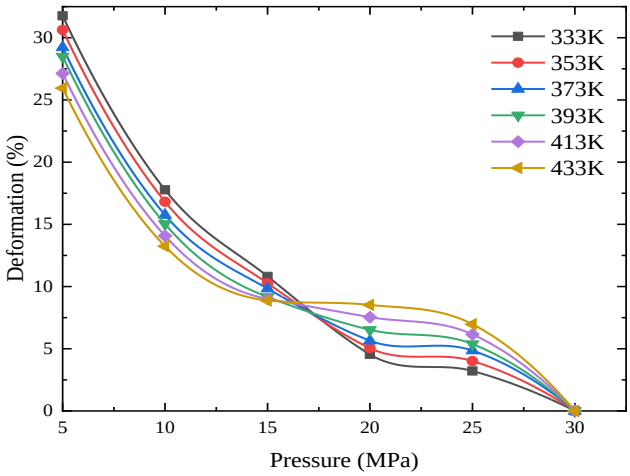

Fig.3 Pore deformation under different temperature

2.3.2 Variation with Pore Diameter

Observations suggest a consistent trend in pore behavior under different pore diameters: as the pressure decreases or the pressure difference from the initial 30MPa increases, the molecules adsorbed on the wall desorb, transforming into a free state and thus increasing the deformation amount. For instance, under a pressure of 15MPa in a 10nm pore, the pore is 10.84 nm, while at 5MPa, the model pore diameter changes to 11.54 nm. Similarly, in a 2nm pore under 15MPa, the pore measures 2.02nm, whereas at 5MPa, the model pore diameter changes to 2.19nm. Hence, during oil and gas development, as the pressure decreases and shale oil precipitates, the increase in pore diameter positively affects subsequent production processes, and the deformation rate gradually increases over time.

Simultaneously, as the initial pore diameter increases, the magnitude of pore deformation also increases. For example, the deformation at 5MPa in a 10nm pore is 29.22%, in a 6nm pore is 20.80%, while it is 9.62% in a 2nm pore, decreasing by 67.07% compared to a 10nm pore and 53.75% compared to a 6nm pore. In the 15MPa-30MPa interval, the deformation differences corresponding to different pore diameters are not significant, while in the 5MPa-15MPa interval, the deformation curve steeply increases. This suggests that during desorption, as the pressure decreases, the adsorption quantity of multi-component gas in shale slowly decreases. Once the pressure decreases below 15MPa, further pressure reduction causes a rapid decrease in adsorption quantity, leading to a swift increase in shale deformation. Therefore, the trend of the deformation quantity is largely similar to the desorption curve.

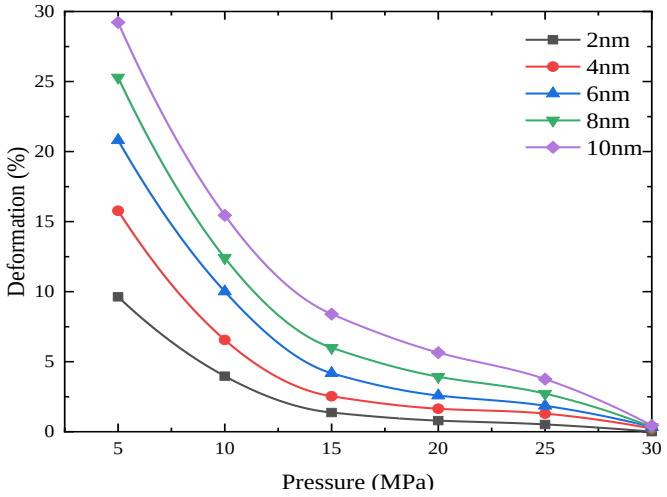

Fig.4 Pore deformation under different pore sizes

2.3.3 Variation with Proportion

From Fig.5, one can infer the relationship between deformation at 373K and the component proportions in the shale reservoir. When component ratios change, the general trend is similar, with the deformation order being 3:1>1:1>1:3 (CO_2:CH_4), i.e., when CO_2 has the highest proportion, deformation exceeds other proportions. The maximum deformation under different ratios all occur at 5MPa. At 1:1, the maximum deformation is 29.22%, at 1:3, the maximum deformation is 24.97%, and when the ratio changes to 3:1, the maximum deformation reaches 32.99%, an increase of 12.9% compared to 1:1, and 32.12% compared to 1:3. Therefore, when the mole fraction of CO_2 increases from 0.25 to 0.75, the maximum volume strain induced by the mixed component adsorption first shows an increasing trend. This is because compared to methane, carbon dioxide has a stronger adsorption capacity in shale. The total adsorption quantity of mixed components increases with the increase of carbon dioxide mole fraction, thereby generating greater volume strain. Similarly, in the 15MPa-30MPa interval, the deformation differences corresponding to different pore diameters are not significant, while in the 5MPa-15MPa interval, the deformation curve steeply increases.

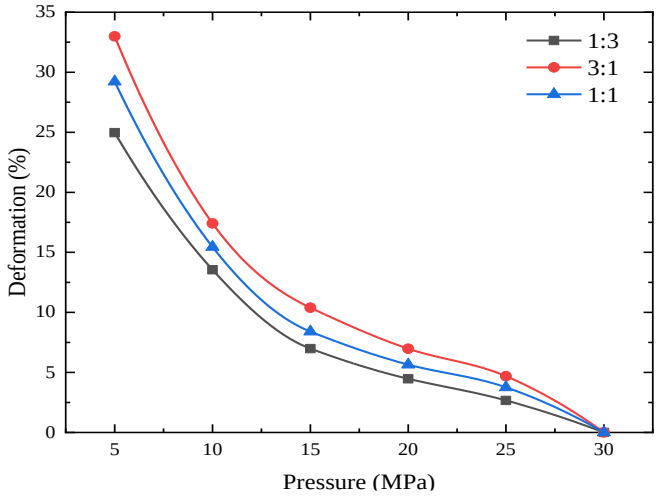

Fig.5 Pore deformation under different pore ratios

3. MECHANISMS OF MIXED GAS MIGRATION IN INORGANIC NANOPORES

3.1 Model Development

3.1.1 Basic Assumptions

Considering the complex geological conditions of shale gas, the migration of gas in the inorganic nanopores of shale is influenced by numerous factors. However, it's unfeasible to incorporate all these factors in constructing the migration process. Therefore, when establishing the mathematical model for

multicomponent gas migration in inorganic nanopores, factors such as the presence of CO_2, CH_4 and bound water must be contemplated, and reasonable assumptions made. The assumptions are as follows:

(1) It is assumed that there are multiple capillaries of the same diameter and parallel arrangement in the shale reservoir;

(2) The pores contain a variety of component fluids, including CO_2, CH_4, and H_2O;

(3) The adsorption of other gas components is ignored due to the presence of an adsorbed water film;

(4) The water film is incompressible;

(5) The dissolution of gas components CO_2 and CH_4 in the water film is disregarded;

(6) The gas seepage process is assumed to be isothermal;

(7) The effect of gravity is ignored.

3.1.2 Mathematical Model

The Knudsen number is the ratio of the average molecular mean free path of the gas to the characteristic length of the pore, expressed as:

$$Kn = \frac{\lambda}{D} \qquad (1)$$

Where, λ represents the average molecular mean free path (nm), and D represents the characteristic length is the pore diameter (nm).

The Knudsen number is a function of the gas average molecular mean free path and the pore diameter. Changes in these two parameters lead to a change in the gas migration mechanism, that is, a change in the state of gas migration in nanopores. By adjusting these two parameters, the Knudsen number can be corrected.

To obtain the actual pore diameter, it's necessary to consider the effective gas migration channel. Under the effect of effective pore stress, the pore diameter changes. In inorganic nanopores, due to the hydrophilicity of clay minerals, water molecules form a water film on the pore wall, changing the pore diameter.

In the depressurization development of shale gas, when the confining pressure is fixed, the effective pore stress increases as the pore pressure decreases, leading to a change in the pore space due to stress deformation, reducing the effective gas migration channel. Stress deformation leads to a reduction in shale permeability, porosity, and pore diameter. Compared to conventional reservoirs, *unconventional reservoirs, especially those at the nanoscale in shale, are more greatly influenced by stress deformation effects.*

Dong et al. carried out shale stress deformation test experiments, established the relationship between the intrinsic permeability of shale, porosity, and pressure, and demonstrated that the stress deformation effect on the intrinsic permeability and porosity of shale can be represented by a power law relationship , which is:

$$K = K_o \left(P_e / P_o\right)^{-s} \qquad (2)$$

$$\phi = \phi_o \left(P_e / P_o\right)^{-q} \qquad (3)$$

Where, K represents the permeability of shale under effective stress (m^2), P_e represents the intrinsic permeability of shale under atmospheric pressure (m^2), P_o symbolizes effective stress (MPa), ϕ represents atmospheric pressure (MPa), ϕ_o represents the porosity of shale under effective stress (dimensionless), represents the porosity of shale under atmospheric pressure (dimensionless), s represents the stress deformation coefficient of shale permeability (dimensionless), and q represents the stress deformation coefficient of shale porosity (dimensionless).

The effective pore stress is expressed as:

$$P_e = P_c - \chi P \qquad (4)$$

Where, P_c represents the external confining pressure of the pore (MPa), P is the internal pressure of the pore (MPa), and χ represents the Biot coefficient, valued at 1.

Based on the Hagen-Poiseuille theory, the relationship between shale nanopore radius, permeability, and porosity is expressed as:

$$K_o = \frac{\phi_o r_o^{\,2}}{8} \qquad (5)$$

Where, r_o represents the initial pore radius of shale pores (nm).

Substituting equations (2) and (3) into equation (5), we obtain the radius of multicomponent gas migration in shale inorganic nanopores under the influence of stress deformation, which is expressed as:

$$r_{iom} = r_o \left(P_e / P_o\right)^{0.5\,q-s} \qquad (6)$$

Where, r_{iom} represents the pore radius under effective stress in shale inorganic nanopores (nm).

Based on considering the effects of stress deformation, considering the impact of bound water (water film) on the migration radius of the pore, we obtain the effective migration radius of multicomponent gas in shale inorganic nanopores, expressed as:

$$r_{\text{e-iom}}=r_{\text{iom}}-\delta=r_{\text{o}}\left(P_{\text{e}}/P_{\text{o}}\right)^{0.5\,q\text{-}s}-\delta \quad (7)$$

Where, δ represents the thickness of the water film (nm). This study considers a homogeneous model, where the water film is evenly distributed on the pore wall, the water saturation is less than 1, and the thickness of the water film is referenced to the second chapter of this paper.

The effective porosity of shale inorganic nanopores influenced by stress deformation and bound water (water film) effects is represented as:

$$\phi_{\text{e-iom}}=\phi_{\text{o}}\frac{r_{\text{e-iom}}^2}{r_{\text{o}}^2}=\phi_{\text{o}}\frac{\left[r_{\text{o}}\left(P_{\text{e}}/P_{\text{o}}\right)^{0.5\,q\text{-}s}-\delta\right]^2}{r_{\text{o}}^2} \quad (8)$$

Where, $\phi_{\text{e-iom}}$ represents the effective porosity (dimensionless), and $r_{\text{e-iom}}$ represents the effective pore radius (nm).

To obtain the true average molecular mean free path, it's necessary to consider the average molecular mean free path under the condition of multicomponent gas migration. Shale gas is a mixture of multiple gases such as CH_4, C_2H6, and CO_2, migrating in real shale nanopores. Previous studies did not consider this reality and only considered the migration situation of single component gas CH4 and two components CO_2/CH_4.

Given the compressibility of gases, the real gas effect needs to be considered. Civan et al. proposed taking into account the real gas effect, introducing the gas compressibility factor to calculate the average molecular mean free path, which is expressed as:

$$\lambda=\frac{\mu}{P}\sqrt{\frac{\pi ZRT}{2M}} \quad (9)$$

Where, μ represents the gas viscosity (Pa·s), P represents pore pressure (MPa), Z represents the gas compressibility factor (dimensionless), M represents the molar mass of the gas (kg/mol), R designates the gas constant (J/(mol·K)), and T represents the formation temperature (K).

The gas compressibility factor is a function of shale pore pressure and temperature, illustrating the relationship between real gas and ideal gas based on the critical properties of gas. It can be expressed as:

$$Z=0.702e^{-2.5T_{pr}}P_{pr}^2-5.524e^{-2.5T_{pr}}P_{pr}+0.044T_{pr}^2-0.164T_{pr}+1.15 \quad (10)$$

$$P_{pr}=\frac{P}{P_c} \quad (11)$$

$$T_{pr}=\frac{T}{T_c} \quad (12)$$

Where, P_{pr} represents the comparative pressure of the gas (dimensionless), T_{pr} represents the comparative temperature of the gas (dimensionless), P_c represents the critical pressure (MPa), and T_c represents the critical temperature (K). Under the same conditions of comparative pressure and temperature, the compressibility factor of various gases is identical.

According to formula (8), the average molecular mean free path of a multicomponent gas mixture in inorganic nanopores can be obtained, expressed as:

$$\lambda_{\text{mix}}=\frac{\mu_{\text{mix}}}{P}\sqrt{\frac{\pi Z_{\text{mix}}RT}{2M_{\text{mix}}}} \quad (13)$$

Where, λ_{mix} represents the average molecular mean free path of the multicomponent gas mixture (nm), μ_{mix} represents the viscosity of the multicomponent gas mixture (Pa·s), M_{mix} represents the molar mass of the multicomponent gas mixture (kg/mol), and Z_{mix} represents the compressibility factor of the multicomponent gas mixture (dimensionless).

According to formulas (1), (7), and (13), the Knudsen number of a multicomponent gas mixture in inorganic nanopores can be obtained, expressed as:

$$Kn_{\text{iom}}=\frac{\lambda_{\text{mix}}}{2r_{\text{e-iom}}}=\frac{\frac{\mu_{\text{mix}}}{P}\sqrt{\frac{\pi Z_{\text{mix}}RT}{2M_{\text{mix}}}}}{2\left[r_{\text{o}}\left(P_{\text{e}}/P_{\text{o}}\right)^{0.5\,q\text{-}s}-\delta\right]} \quad (14)$$

3.2 Mathematical Model of Multicomponent Gas Migration in Inorganic Nanopores

Molecular simulation and experimental studies demonstrate that water molecules exist in the form of a water film on the surface of inorganic nanopores, resulting in a reduced pore migration radius and gas transportation capacity. Due to the strong hydrophilicity of clay minerals, the water film rarely participates in the fluid migration process under lower pressure gradients. Therefore, gas in inorganic nanopores only undergoes phase migration, including continuous flow, slip flow, and Knudsen diffusion.

3.2.1 Mathematical Model of Multicomponent Gas Slip Flow

In shale inorganic nanopores, when the pore size is significantly larger than the average molecular free path of the gas, specifically, when Kn≤10-3, gas migration in shale inorganic nanopores is predominantly due to inter-molecular collisions. Collisions between molecules and the pore wall can be neglected, and gas migration occurs through Darcy flow under the influence of a pressure gradient. It can be described by the Darcy equation, with the mass flow rate of continuous flow expressed as:

$$J_D = -\mathrm{K}_\infty \frac{\rho}{\mu}\nabla P = -\frac{\phi r^2 \rho}{8\mu}\nabla P \quad (15)$$

$$\nabla P = \frac{\Delta P}{L} \quad (16)$$

Where, J_D represents the mass flow rate of slip flow at the no-slip boundary under the influence of a pressure gradient (kg/(m^2·s)), K_∞ represents the inherent permeability of the porous medium (m^2), ϕ represents porosity (dimensionless), μ represents gas viscosity (Pa·s), ρ represents gas density (kg/m^3), P represents pore pressure (MPa), r represents pore radius (nm), and L represents pore length (nm).

When the pore size of shale inorganic nanopores is larger than the average molecular free path of the gas, that is, when 10^{-3}<Kn≤10^{-1}, not only must the influence of inter-molecular collisions on gas migration be considered, but also the impact of collisions between gas molecules and the pore wall. In this scenario, slip effects occur on the pore wall.

Based on the Beskok-Karniadakis (B-K) model, the slip boundary correction coefficient is introduced and expressed as:

$$f\ K_n = 1+\alpha K_n \left(1+\frac{4K_n}{1-bK_n}\right) \quad (17)$$

Where, b represents the slip constant (dimensionless). For first-order slip boundary conditions, the b value is set to 0. For second-order slip boundary conditions, the b value is set to -1. α represents the rarefaction effect coefficient (dimensionless).

According to the empirical fitting formula, the gas rarefaction effect coefficient can be expressed as:

$$\alpha = \frac{128}{15\pi^2}\tan^{-1}\ 4Kn^{0.4} \quad (18)$$

Based on the aforementioned formula, the corrected slip coefficient for the multicomponent gas is expressed as:

$$f\ Kn_{\mathrm{iom}} = 1+\alpha_{\mathrm{iom}} Kn_{\mathrm{iom}} \left(1+\frac{4Kn_{\mathrm{iom}}}{1-bKn_{\mathrm{iom}}}\right) \quad (19)$$

$$\alpha_{\mathrm{iom}} = \frac{128}{15\pi^2}\tan^{-1}\ 4Kn_{\mathrm{iom}}^{0.4} \quad (20)$$

Following the formulas (20), (21), (22), and (23), the mass flow rate of multicomponent gas slip flow in inorganic nanopores can be obtained, expressed as:

$$J_{v\text{-iom}} = -\frac{\phi_{e\text{-iom}}}{\tau}\frac{r_{e\text{-iom}}^2}{8}\frac{\rho_{\mathrm{iom}}}{\mu_{\mathrm{iom}}}\ 1+a_{\mathrm{iom}}Kn_{\mathrm{iom}} \left(1+\frac{4Kn_{\mathrm{iom}}}{1-bKn_{\mathrm{iom}}}\right)\nabla P \quad (21)$$

Based on the definition of permeability, the mass flow rate is converted into equivalent permeability:

$$K = -\frac{J\mu}{\rho\nabla P} \quad (22)$$

Based on formulas (21) and (22), the permeability of the multicomponent gas slip flow in inorganic nanopores can be obtained, expressed as:

$$K_{v\text{-iom}} = \frac{\phi_{e\text{-iom}}}{\tau}\frac{r_{e\text{-iom}}^2}{8}\ 1+a_{\mathrm{iom}}Kn_{\mathrm{iom}} \left(1+\frac{4Kn_{\mathrm{iom}}}{1-bKn_{\mathrm{iom}}}\right) \quad (23)$$

3.2.2 Multicomponent Gas Knudsen Diffusion Mathematical Model

When the pore size of shale is on the same order of magnitude as the average molecular free path of gas, that is, when 10^{-1}＜Kn≤10^{1}, inter-molecular collisions between gas molecules and the pore wall exert a

significant influence on gas migration. In this case, the Knudsen diffusion of gas needs to be considered. The mass flow rate caused by Knudsen diffusion is represented by the Knudsen equation：

$$J_k = -MD_k \nabla C \quad (24)$$

Where, J_k represents the Knudsen diffusion mass flow rate (kg/(m^2·s)); C represents the gas concentration (mol/m^3); D_k represents the Knudsen diffusion coefficient (m^2/s).

The gas concentration can be expressed as:

$$C = \frac{P}{ZRT} \quad (25)$$

The Knudsen diffusion coefficient for shale nanopores is expressed as:

$$D_k = \frac{2r}{3}\sqrt{\frac{8RT}{\pi M}} \quad (26)$$

Based on the above formula, the Knudsen diffusion coefficient for the multicomponent gas can be expressed as:

$$D_{k\text{-mix}} = \frac{2r_{\text{e-iom}}}{3}\sqrt{\frac{8RT}{\pi M_{\text{mix}}}} \quad (27)$$

Based on the aforementioned formulas (25), (26), (27), the Knudsen diffusion mass flow rate for multicomponent gases in inorganic nanopores can be obtained, expressed as：

$$J_{k\text{-iom}} = -\frac{\phi_{\text{e-iom}}}{\tau}\frac{2r_{\text{e-iom}}}{3}\sqrt{\frac{8M_{\text{mix}}}{\pi RT}}\nabla P \quad (28)$$

Based on formulas (22) and (28), the permeability of Knudsen diffusion for multicomponent gases in inorganic nanopores can be obtained, expressed as:

$$K_{\text{k-iom}} = \frac{\phi_{\text{e-iom}}}{\tau}\frac{2r_{\text{e-iom}}\mu_{\text{mix}}}{3}\sqrt{\frac{8RT}{\pi M_{\text{mix}}}} \quad (29)$$

3.2.3 Multicomponent Gas Bulk Apparent Permeability Model

In this section, based on the weight coefficients proposed by Wu et al., the permeability of slip flow and Knudsen diffusion are superimposed to obtain the bulk apparent permeability model for multicomponent gases in inorganic nanopores, expressed as:

$$K_{t\text{-iom}} = \omega_{v\text{-iom}}K_{v\text{-iom}} + \omega_{k\text{-iom}}K_{k\text{-iom}} \quad (30)$$

Where, $\omega_{v\text{-iom}}$ represents the weight coefficient of slip flow permeability for multicomponent gases in inorganic nanopores (dimensionless); $K_{v\text{-iom}}$ represents the slip flow permeability for multicomponent gases in inorganic nanopores (m^2); $\omega_{k\text{-iom}}$ represents the weight coefficient of Knudsen diffusion permeability for multicomponent gases in inorganic nanopores (dimensionless); $K_{k\text{-iom}}$ represents the Knudsen diffusion permeability for multicomponent gases in inorganic nanopores (m^2). The weight coefficient of slip flow permeability for multicomponent gases in inorganic nanopores is expressed as:

$$\omega_{v\text{-iom}} = \frac{1}{1+Kn_{\text{iom}}} = \frac{1}{1+\dfrac{\dfrac{\mu_{\text{mix}}}{P}\sqrt{\dfrac{\pi Z_{\text{mix}}RT}{2M_{\text{mix}}}}}{2\left[r_{\text{o}}\ \ P_{\text{e}}/P_{\text{o}}\ ^{0.5\ q\text{-}s} - \delta\right]}} \quad (31)$$

The weight coefficient of Knudsen diffusion permeability for multicomponent gases in inorganic nanopores is expressed as:

$$\omega_{k\text{-iom}} = \frac{1}{1+1/Kn_{\text{iom}}} = \frac{1}{1+\dfrac{2\left[r_{\text{o}}\ \ P_{\text{e}}/P_{\text{o}}\ ^{0.5\ q\text{-}s} - \delta\right]}{\dfrac{\mu_{\text{mix}}}{P}\sqrt{\dfrac{\pi Z_{\text{mix}}RT}{2M_{\text{mix}}}}}} \quad (32)$$

Since only bulk free gas exists in inorganic nanopores, the apparent permeability of CO^2-multicomponent gas in inorganic nanopores is the bulk apparent permeability. Based on the aforementioned formulas (23), (29), (31), and (32), it is expressed as:

$$K_{\text{iom}} = \omega_{v\text{-iom}}K_{v\text{-iom}} + \omega_{k\text{-iom}}K_{k\text{-iom}} \quad (33)$$

3.3 Results Analysis

3.3.1 Contributions from Different Migration Mechanisms

（1）Slip Flow

As can be observed from the fig.6, with the increase in pore size, the proportion of gas slip flow permeability increases, and the contribution from slip flow becomes more significant. When the pore pressure is 30MPa and the pore diameter is 10nm, the proportion of slip flow permeability tends towards 100%; when the pore pressure is 5MPa and the pore diameter is 2nm, the proportion of slip flow permeability tends towards 20%, indicating that slip flow plays a dominant role under high pressure and large pore diameter conditions. This is because the larger the pore size, the larger the proportion of gas movement via molecular collisions; the higher the pressure, the higher the frequency of molecular collisions. Under 2nm pore size, the frequency of collisions between molecules and the wall increases, and although the frequency of molecular collisions significantly decreases, it still constitutes a considerable proportion, indicating that the sensitivity of slip permeability to pressure and pore size far exceeds that of Knudsen diffusion permeability.

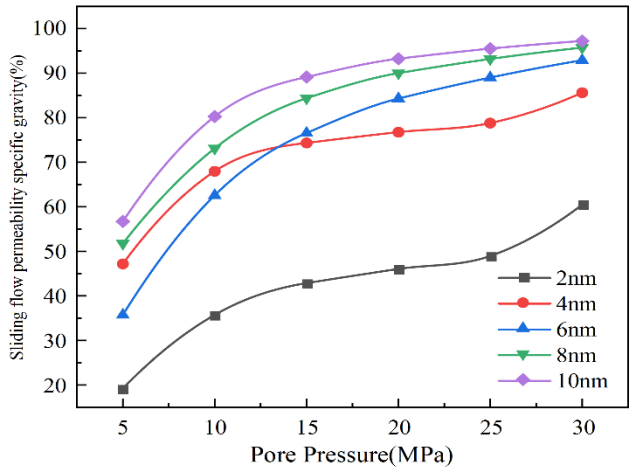

Fig.6 Slip flow penetration, metaphorically weight changes with pore pressure

（2）Knudsen Diffusion

As depicted in the fig.7, as the pore pressure decreases, the proportion of Knudsen diffusion permeability gradually increases, and the contribution of Knudsen diffusion to apparent permeability becomes more significant. With the increase in pore size, the proportion of gas Knudsen diffusion permeability decreases, and the contribution of Knudsen diffusion becomes less significant. When the pore pressure is 5MPa and the pore diameter is 2nm, the proportion of Knudsen diffusion permeability tends towards 80%; when the pore pressure is 30MPa and the pore diameter is 10nm, the proportion of Knudsen diffusion permeability tends towards 0, indicating that Knudsen diffusion plays a dominant role under low pressure and small pore diameter conditions. This is because the smaller the pore size, the higher the probability of molecular collisions with the wall; the lower the pore pressure, the stronger the stress deformation, leading to smaller pore sizes.

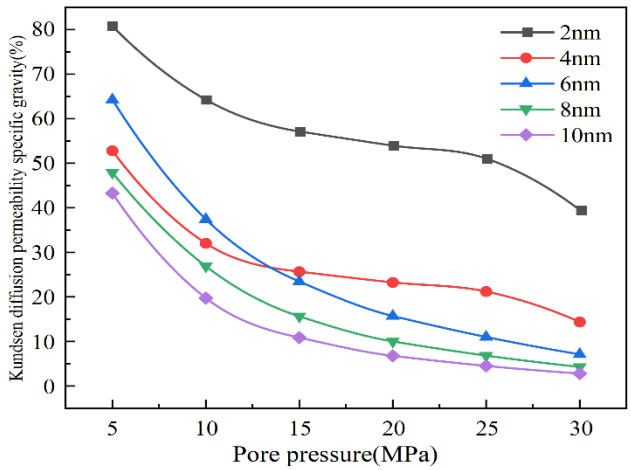

Fig.7 Knudsen diffusion permeability is consumed by pore pressure

3.3.2 Different Pore Sizes

As shown in the fig.8, the apparent permeability first decreases and then increases with the decrease in pore pressure. This is because under high pore pressure conditions, the stress deformation effect enhances with the increase in pore pressure; while under low pore pressure conditions, the gas slip effect and the gas rarefaction effect weaken with the increase in pore pressure. As the pore size increases, the apparent permeability gradually increases. When the pore size is 2nm and 4nm, the change in the bulk apparent permeability of the gas with the decrease in pore pressure is small. In small-sized pores, slip is weakened, and Knudsen diffusion does not effectively enhance, resulting in weak gas transport capacity, reducing sensitivity to pressure. When the pore size exceeds 10nm, the apparent permeability increases significantly, with a sudden increase in permeability. This is because in inorganic nanopores, due to the presence of a water film, the effective migration channel is reduced. The influence of the water film is strong in small-sized pores, while it weakens in large-sized pores.

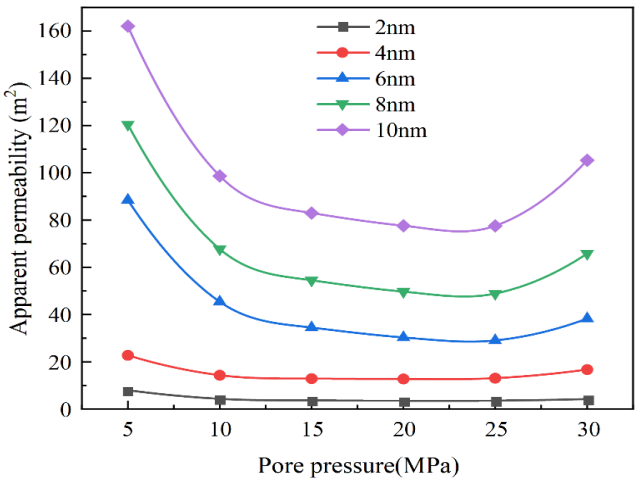

Fig.8 Effect of pore size ratio on table permeability

3.3.3 Different Proportions

As seen from the fig.9, when the component ratio of the multi-component gas CO_2 and CH4 is 1:3, i.e., the mole fraction of CO_2 is 25%, the apparent permeability is at its peak; when the component ratio is 3:1, i.e., the mole fraction of CO_2 is 75%, the apparent permeability is at its lowest. With the increase in the mole fraction of CO_2, the apparent permeability gradually decreases. The diameter of CO_2 molecules is larger than that of CH_4, and the collision frequency between large-diameter molecules is lower than that of small-diameter ones, thus the greater the mole fraction of CO_2, the lower the apparent permeability.

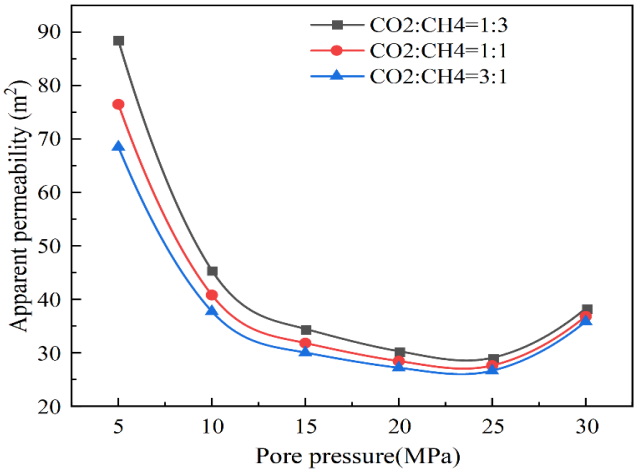

Fig.9 Effect of component ratio on table reference permeability

4 CONCLUSIONS

The adsorption of mixed gases in organic nanopores leads to further deformation of the pores, and there are significant differences in the variation of pore deformation under different temperature, pore size, and ratio conditions. The gas migration in nanopores faces substantial resistance, and the mobility of the gas is relatively poor. This paper clarifies the dynamic process of gas migration in nanopores, reveals the resistance response mechanism in the process of gas migration, and analyzes the effects of factors such as water film thickness and gas-water interface tension on capillary pressure. The results show:

(1) The deformation is greater when the proportion of CO_2 is the highest than in other proportions, and the maximum deformation in different proportions occurs at 5MPa. As the initial pore size increases, the magnitude of pore deformation also increases.

(2) Gas-solid interaction and capillary pressure are the main reasons that hinder the migration of multi-component gas in shale inorganic nanopores.

(3) When the pore size is less than or equal to 2nm, the driving force cannot balance with the gas migration resistance, leading to unstable gas migration and difficulties in gas flow. When the pore size is greater than 8nm, the resistance to gas migration mainly comes from capillary pressure, whereas for less than 8nm, it is elevated by both capillary pressure and gas-solid interaction. Moreover, as the pore size decreases, the contribution of gas-solid interaction to migration resistance increases.

ACKNOWLEDGEMENT

The authors would like to appreciate the financial support of the National Natural Science Foundation of China [No. 52004038], Study on the Microscopic Phase Behavior and Migration Mechanism of CO_2 and Multicomponent Alkanes in Shale Dynamical Nanopore.

DECLARATION OF INTEREST STATEMENT

The authors declare that they have no known competing financial interests or personal relationships that could have appeared to influence the work reported in this paper. All authors read and approved the final manuscript.

REFERENCE

[1] Lei Chen,Zhenxue Jiang,Qingxin Liu,Shu Jiang,Keyu Liu,Jingqiang Tan,Fenglin Gao. Mechanism of shale gas occurrence: Insights from comparative study on pore structures of marine and lacustrine shales[J]. Marine and Petroleum Geology,2019,104.

[2] An Wang, Guodong Qi, "Study on Two-phase Flow Mechanisms in Nanopore Considering Microcosmic Deformation and Dynamic Capillary Force", Geofluids, vol. 2022, Article ID 7485271, 13 pages, 2022.

[3] A. A. Fomkin,A. V. Shkolin,A. L. Pulin,I. E. Men’shchikov,E. V. Khozina. Adsorption-Induced Deformation of Adsorbents[J]. Colloid Journal,2018,80(5).